Seismic Response of Yielding Multistory Steel Buildings Equipped with Pressurized Sand Dampers

Gholamreza Moghimi, S.M.ASCE[1]; and Nicos Makris, F.ASCE[2]

Abstract: This paper investigates the seismic response analysis of the 9-story SAC building equipped with pressurized sand dampers, a new type of low-cost energy dissipation device where the material enclosed within the damper housing is pressurized sand. The strength of the pressurized sand damper is proportional to the externally exerted pressure on the sand via prestressed steel rods; therefore, the energy dissipation characteristics of a given pressurized sand damper can be adjusted according to a specific application. The strong pinching behavior of pressurized sand dampers was characterized with a previously developed three-parameter Bouc-Wen hysteretic model that for this study was implemented in the open source code OpenSees with a C++ algorithm, and it was used to analyze the seismic response of the 9-story SAC building subjected to six strong ground motions that exceed the design response spectrum for all soil categories. The paper shows that for the family of strong ground motions used in this study, pressurized sand dampers with strength of the order of 5%–10% of the weights of their corresponding floors were able to keep the interstory drifts of the 9-story SAC building at or below 1%, while base shears and peak plastic hinge rotations were reduced in the damped configuration. Supplemental damping produced mixed results on floor accelerations; nevertheless, in most floors, peak accelerations were reduced. **DOI: 10.1061/(ASCE)ST.1943-541X.0003364.** *© 2022 American Society of Civil Engineers.*

Introduction

In the early 1970s a new concept for seismic protection involving modifying the earthquake response of structures with specially designed supplemental energy dissipation devices was brought forward in the seminal papers by Kelly et al. (1972) and Skinner et al. (1974) and was implemented in important structures that were under design at that time, such as the South Rangitikei Rail Bridge (Beck and Skinner 1973; Skinner et al. 1974; Kelly 1997), the Union House Building in Auckland (Boardman et al. 1983), and the Wellington Central Police Station in Wellington (Charleson et al. 1987), New Zealand. The 1972 paper by Kelly et al. marks the beginning of the use of passive energy dissipation (response modification) devices for the seismic protection of structures, devices that today find worldwide applications. Supplemental passive energy dissipation devices enhance the ability of a framed structure to dissipate the earthquake-induced kinetic energy, therefore limiting inelastic structural deformations and damage (Constantinou and Symans 1993; Whittaker et al. 1993). Devices most commonly used for the response modification of structures include viscous fluid dampers, viscoelastic fluid and viscoelastic solid dampers, friction dampers, metallic yielding dampers, and buckling-restrained braces (BRBs) (Soong and Dargush 1997; Constantinou et al. 1998; Hanson and Soong 2001; Black et al. 2002, 2004).

A half century after the first application of supplemental energy dissipation devices (torsionally yielding steel beam dampers) at the stepping piers of the South Rangitikei Rail Bridge (Kelly et al. 1972; Skinner et al. 1980), viscous fluid dampers and BRBs have emerged as the two types of passive energy dissipation devices that today enjoy the widest implementations. Viscous fluid dampers that generate fluid flow through orifices or values were originally developed for shock isolation in military applications, and their technology was gradually transferred to civil applications in the 1980s (Constantinou et al. 1998; Symans et al. 2008). A potential challenge with fluid dampers is whether they can maintain their long-term integrity when placed in civil structures that are subjected to a variety of dynamic displacements ranging from impulsive shocks to prolonged fluctuating displacement histories (Matier and Ross 2013). Early theoretical studies on the problem of viscous heating of fluid dampers have been presented by Makris (1998) and Makris et al. (1998), and they have been confirmed experimentally by Black and Makris (2006, 2007) and have uncovered combinations of internal fluid pressure and number of cycles that may lead to potential failure of fluid dampers due to viscous heating. BRBs are yielding braces that offer supplemental hysteretic energy dissipation while increasing the strength of the structure (Watanabe et al. 1988; Wada et al. 1989; Black et al. 2002, 2003, 2004; FEMA 2006). Because of their distributed yielding that leads to stable hysteretic behavior, BRBs enjoy worldwide acceptance and have been proven to be dependable response modification devices for specific applications where the displacement demands are relatively small (a few centimeters) (Sabelli et al. 2003; Fahnestock et al. 2007).

An innovative, low-cost, long-stroke pressurized sand damper was recently developed and tested by Makris et al. (2021). Given that the material surrounding the moving piston and enclosed within the damper housing is pressurized sand as illustrated in Fig. 1, the pressurized sand damper does not suffer from the challenge of viscous heating and failure of its end seals; therefore, it can be implemented in harsh environments with extreme high or low temperatures as have been recorded in Alaska (−40°F) or in Imperial Valley, California (El Centro: +120°F). Furthermore, its symmetric force output is velocity independent and can be

[1]Doctoral Candidate, Dept. of Civil and Environmental Engineering, Southern Methodist Univ., Dallas, TX 75275. ORCID: https://orcid.org/0000-0001-5950-5204

[2]Professor, Dept. of Civil and Environmental Engineering, Southern Methodist Univ., Dallas, TX 75275 (corresponding author). ORCID: https://orcid.org/0000-0002-9059-2147. Email: nmakris@smu.edu

Note. This manuscript was submitted on June 4, 2021; approved on February 14, 2022; published online on April 18, 2022. Discussion period open until September 18, 2022; separate discussions must be submitted for individual papers. This paper is part of the ***Journal of Structural Engineering***, © ASCE, ISSN 0733-9445.

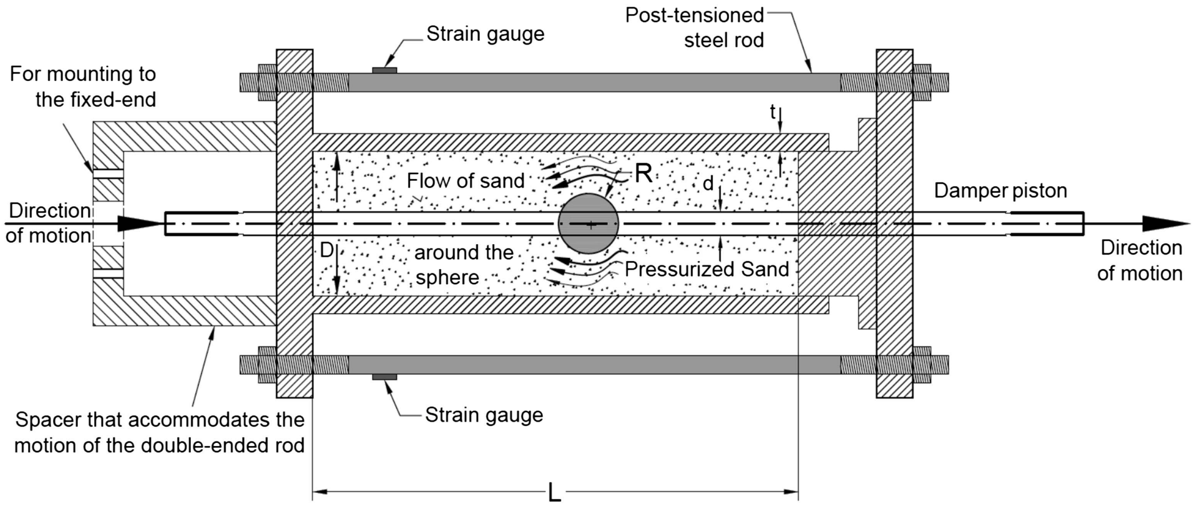

Fig. 1. Schematic of a pressurized sand damper in which energy is dissipated from the shearing action of the sand as the sphere mounted on the damper piston plows through the pressurized sand. The pressure on the sand is exerted with external post-tensioned steel rods so their tensile force can be easily monitored in real time with strain gauges.

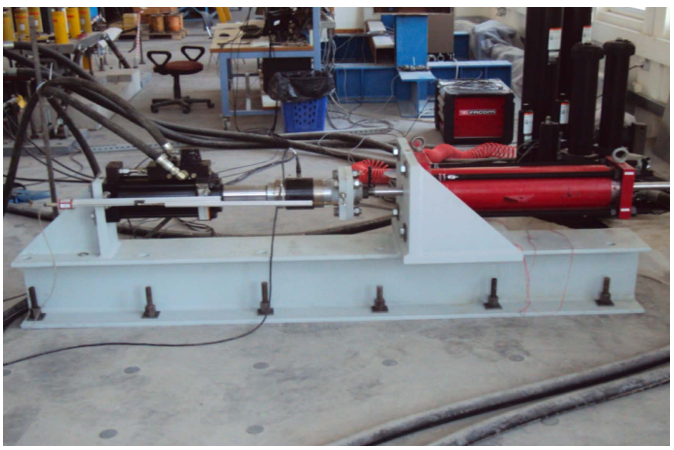

Fig. 2. View of the prototype pressurized sand damper mounted on the experimental setup during cyclic testing at the University of Patras, Greece.

continuously monitored with standard inexpensive strain gauges installed along the post-tensioned rods that exert the pressure on the sand as shown in Fig. 1.

A prototype pressurized sand damper was built and tested in the structures laboratory of the University of Patras, Greece, at various exerted pressures p, stroke amplitudes u_0, and frequencies f_0 by employing the experimental setup shown in Fig. 2 (Makris et al. 2021). Table 1 summarizes the values of pressure, amplitude, and frequency of the cyclic test conducted during the experimental campaigns. Fig. 3 shows selective recorded force-displacement loops from the prototype pressurized sand damper subjected to different pressures and stroke amplitudes. The recorded loops exhibit a repeatable stable behavior with a pronounced pinching that manifests at large strokes. In view of this fail-safe behavior at larger displacement amplitudes in association with the other attractive features of the pressurized sand damper outlined earlier, this paper presents a comprehensive seismic response analysis of the 9-story moment-resisting steel building designed for the SAC Phase II Project (FEMA 2000). This structure that is well known to the

Table 1. Values of the exerted pressure, displacement amplitude, and frequency of the cyclic loading tests

p (MPa)	u_0 (cm)	f_0(Hz)	$v_0 = 2\pi f_0 u_0$ (cm/s)
1, 2, 3, 4, 5	1.0	0.1	0.63
	2.0		1.26
	4.0		2.51
	6.0		3.77
	8.0 (only for $p = 1$ and 2 MPa)		5.02
	10.0 (only for $p = 1$ and 2 MPa)		6.28
	1.0	0.2	1.26
	2.0		2.51
	4.0		5.02
	6.0		7.54
	8.0 (only for $p = 1$ and 2 MPa)		10.05
	10.0 (only for $p = 1$ and 2 MPa)		12.56
	1.0	0.333	2.07
	2.0		4.14
	4.0 (except for $p = 1$ MPa)		8.29
	6.0 (except for $p = 1$ MPa)		12.43
	8.0 (only for $p = 2$ MPa)		16.58
	10.0 (only for $p = 2$ MPa)		20.72
	1.0	0.5	3.14
	2.0		6.28
	4.0 (except for $p = 1$ MPa)		12.56
	6.0		18.84

literature (Gupta and Krawinkler 1998; Chopra and Goel 2002; Aghagholizadeh and Makris 2018) was designed to meet the seismic code (pre-Northridge Earthquake) and represents typical medium-rise buildings designed in the greater area of Los Angeles, California.

Mathematical Model of the Pressurized Sand Damper

Using arguments from dimensional analysis (Langhaar 1951; Barenblatt 1996; Makris and Black 2003a, b) in association with the versatility of the Bouc-Wen model (Wen 1976; Baber and Noori 1985; Constantinou and Adnane 1987; Charalampakis and Koumousis 2008), recently Makris et al. (2021) showed that the

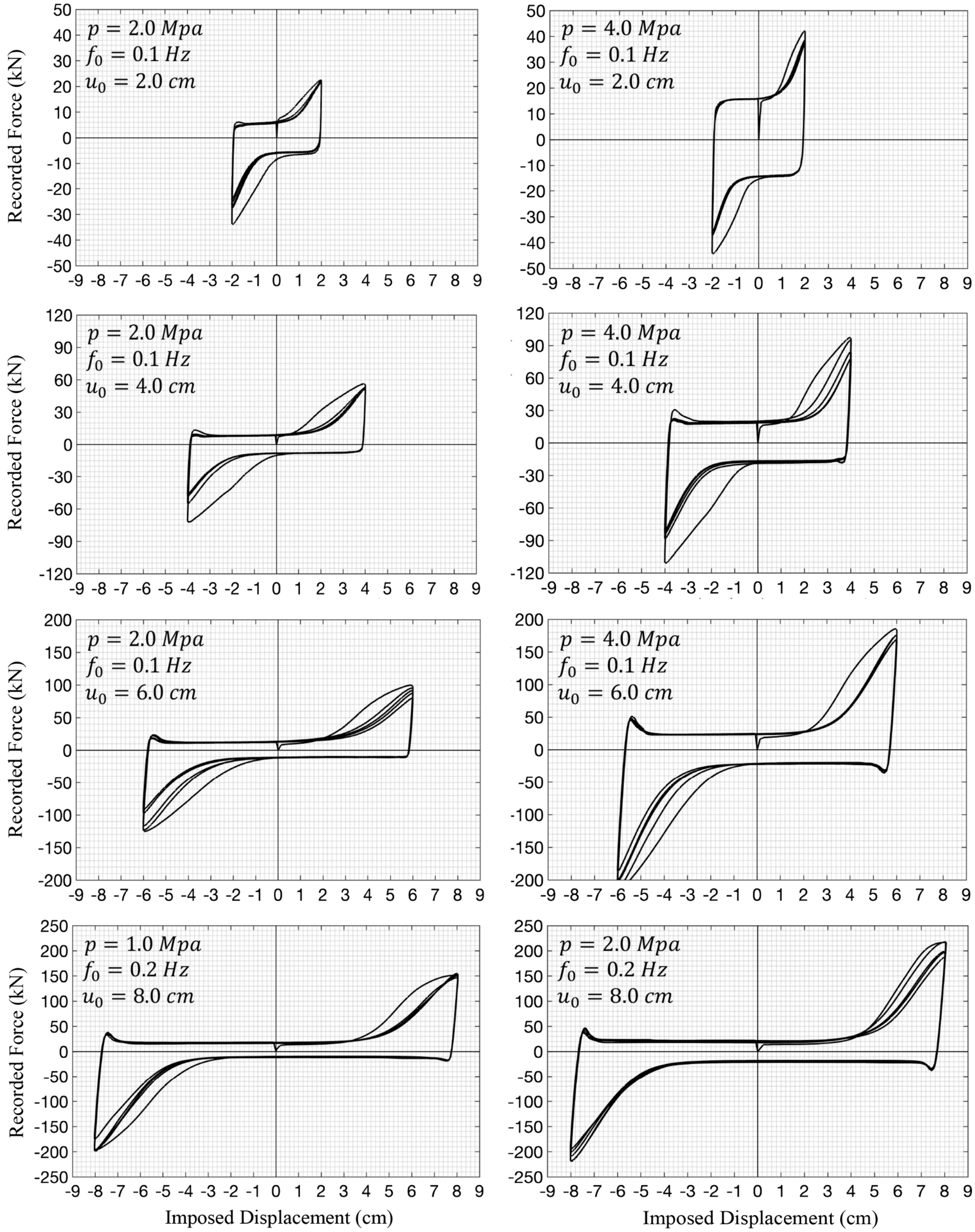

Fig. 3. Selected force-displacement loops of the pressurized sand damper shown in Fig. 2 recorded at various exerted pressures p, stroke amplitudes u_0, and driving frequencies f_0.

strong nonlinear behavior and the pronounced pinching effect at larger strokes of the pressurized sand damper can be satisfactorily approximated with

$$F_d(t) = \Pi_{SD} pR^2[\eta \mathrm{sgn}[\dot{u}(t)] + \zeta z(t)] \tag{1}$$

where $\Pi_{SD} pR^2 = Q$ is the strength of the pressurized sand damper; p = externally exerted pressure on the sand; R = radius of the moving sphere; Π_{SD} = dimensionless damper constant; $\dot{u}(t)$ = velocity of the damper piston; and $z(t)$ = dimensionless internal time-dependent variable of the Bouc-Wen model that is controlled by

$$\dot{z}(t) = \frac{dz(t)}{dt} = \frac{1}{cR}[\dot{u}(t) - \beta \dot{u}(t)|z(t)|^n - \gamma|\dot{u}(t)|z(t)|z(t)|^{n-1}] \tag{2}$$

The exponent n appearing in Eq. (2) controls the transition from the elastic to the yielding regime and is set equal to one ($n = 1$) given that its effect is immaterial. Parameters β and γ control the shape of the hysteretic loop, whereas parameter c expresses the ratio of the yield displacement of the damper to the radius of the sphere R and is set equal to $1/4$ ($c = 0.25$). Parameters η and ζ in Eq. (1) together with parameters β and γ in Eq. (2) are essentially the only four parameters of the proposed model that need to be identified with nonlinear regression analysis (Makris et al. 2021). The hysteretic damper model described by Eqs. (1) and (2) is frequency independent given that the friction stresses that develop along the steel-sphere interface are essentially rate independent.

Fig. 4 plots the measured strength of the damper $Q = \Pi_{SD} pR^2$ that is the output force from the pressurized sand damper during cyclic testing as the sphere mounted on the piston passes by the displacement origin at pressure levels $p = 1.0, 2.0, 3.0, 4.0$, and 5.0 MPa. The data appearing in Fig. 4 include the data initially presented in Makris et al. (2021), together with additional experimental data that were obtained during the course of this study. Linear regression analysis of the recorded data yields a value for the dimensionless damper constant $\Pi_{SD} = Q/pR^2 = 5.12$. In view of the linear dependance of the strength Q to the exerted pressure p [as is suggested by dimensional analysis (Makris et al. 2021)], Fig. 5 plots all the force-displacement loops recorded during our experimental campaigns for all frequencies and exerted external pressures normalized to the strength of the pressurized sand damper $Q = \Pi_{SD} pR^2 = 5.12pR^2$. Given the normalization, at small displacement amplitudes, the normalized damper output force F_d/Q rides essentially along the lines ± 1, therefore parameter η is set equal to one ($\eta = 1$) and the hysteretic (rate-independent) model described by Eqs. (1) and (2) reduces to a three-parameter model in which only parameters ζ, β, and γ need to be identified from nonlinear regression analysis.

Fig. 6 plots the performance of the calibrated hysteretic model described by Eqs. (1) and (2) to capture the overall recorded

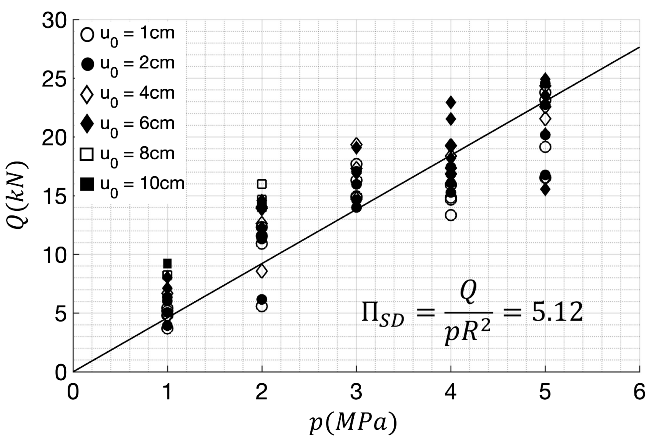

Fig. 4. Measured force from the pressurized sand damper during cyclic testing as the sphere passes by the displacement origin at pressure levels $p = 1.0, 2.0, 3.0, 4.0$, and 5.0 MPa.

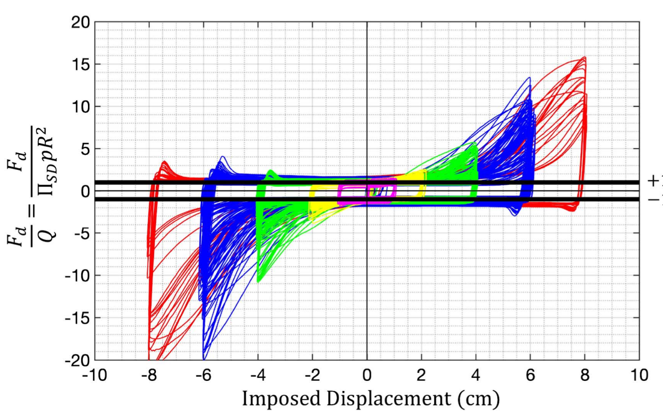

Fig. 5. Recorded force-displacement loops at various amplitudes, exerted pressures, and frequencies normalized to the strength of the pressurized sand damper $Q = 5.12pR^2$. At midstroke [$u(t) = 0$], all recorded loops exhibit essentially the same normalized strength, showing that the force output of the pressurized sand damper is rate independent.

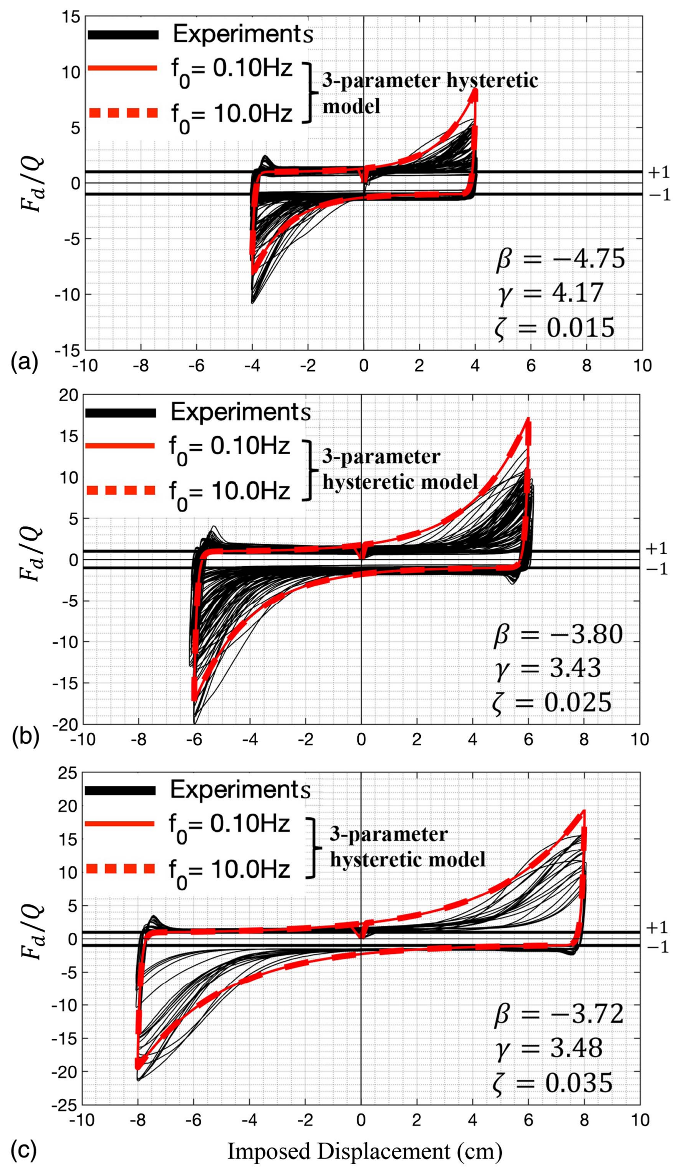

Fig. 6. Normalized force-displacement loops to the strength of the pressurized sand damper: $Q = \Pi_{SD} pR^2$ recorded at all exerted pressures and all cyclic frequencies for stroke amplitudes: (a) ± 4; (b) ± 6; and (c) ± 8 cm (solid lines). Predictions of the three-parameter (ζ, β, and γ) hysteretic model described by Eqs. (1) and (2) with frequencies $f_0 = 0.10$ Hz (thin solid lines) and $f_0 = 10.0$ Hz (heavy dashed lines).

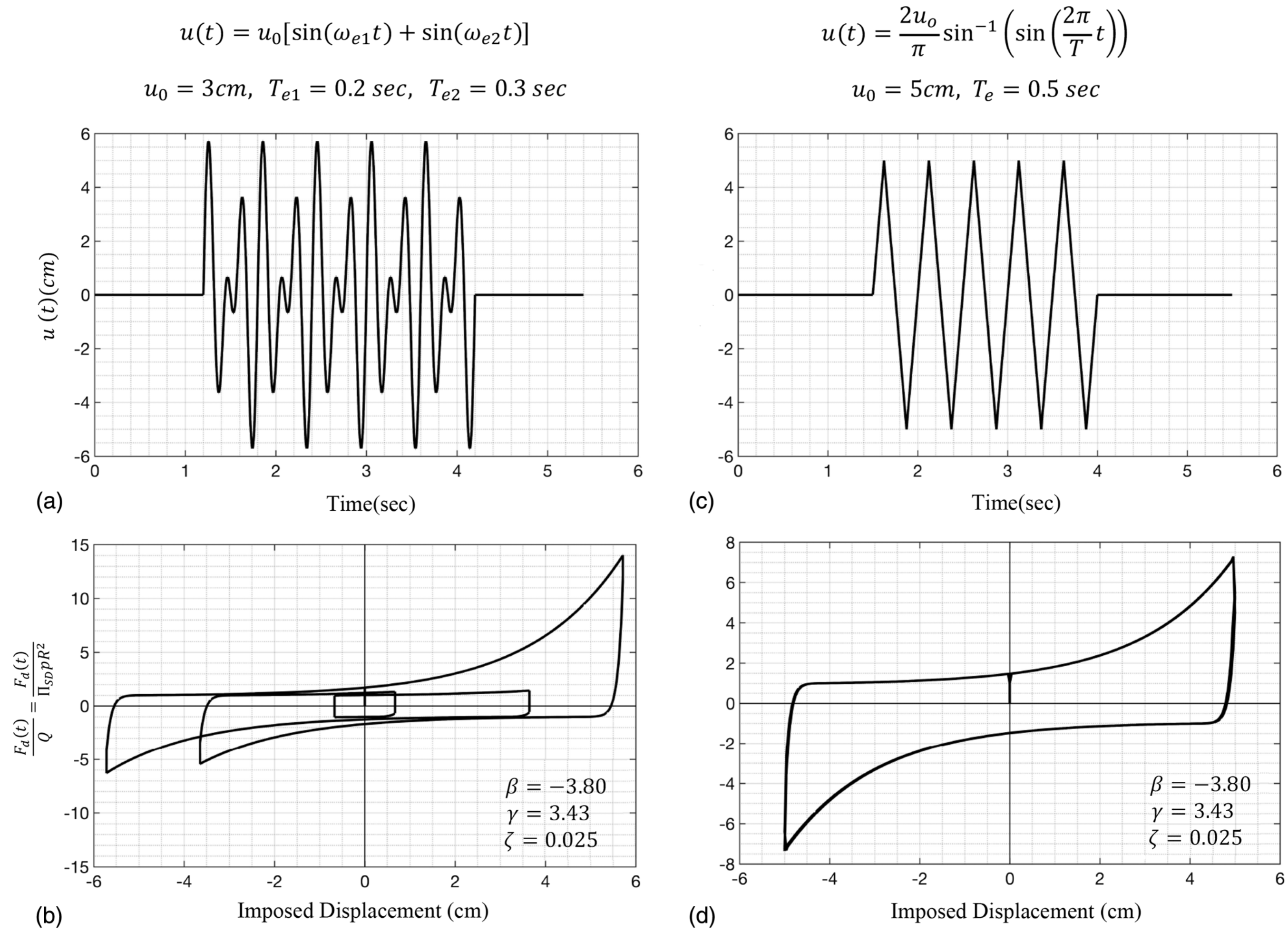

Fig. 7. (a) Periodic displacement history where successive peak negative and positive displacements are not symmetric; and as a result (b) the force-displacement loop that results from Eqs. (1) and (2) is not symmetric. In contrast, (c) when the imposed displacement history is symmetric; and (d) the resulting force-displacement loop is also symmetric.

behavior (at all pressures and all frequencies) as the pressurized sand damper undergoes cyclic motion with displacement amplitudes $u_0 = 4.0, 6.0$, and 8.0 cm. The optimal values of the parameters ζ, β, and γ of the nonlinear hysterics model that resulted from nonlinear regression analysis that best fit the entire families of all the recorded force-displacement loops with stroke amplitude $u_0 = 4.0, 6.0$, and 8.0 cm are shown in each subplot. When both displacement and velocity histories are symmetric, the hysteretic model described by Eqs. (1) and (2) is rate independent.

Fig. 7(a) plots the force-displacement loop as generated by Eqs. (1) and (2) with model parameters $\beta = -3.80$, $\gamma = 3.43$, and $\xi = 0.025$ when the input displacement history contains two distinct excitations frequencies, ω_{e1} and ω_{e2}, and is described by

$$u(t) = u_0[\sin(\omega_{e1}t) + \sin(\omega_{e2}t)] \tag{3}$$

Eq. (3) produces a periodic displacement history; nevertheless, successive peak negative and positive displacements are not symmetric, as shown in Fig. 7(a). In this case the resulting force-displacement loop in Fig. 7(b) ($\omega_{e1} = 2\pi/T_{e1} = 2\pi/0.2s$ and $\omega_{e2} = 2\pi/T_{e2} = 2\pi/0.3s$) is not symmetric. Such a nonsymmetric response, which results from the negative value of parameter β, is known to the literature (Foliente et al. 1996; Ma et al. 2004). In contrast, when the imposed displacement history on the damper is symmetric, as is the triangular displacement input ($u(t) = \frac{2u_o}{\pi}\sin^{-1}(\sin\frac{2\pi}{T_e}t)$) shown in Fig. 7(c), the resulting force-displacement loop is symmetric as shown in Fig. 7(d).

The reason that the optimal values of parameters ζ, β, and γ depend on the stroke amplitude u_0 is due to a first-passage effect that is similar to the scragging effect in elastomeric bearings where larger values of bearing stiffness are observed in the first half-cycle

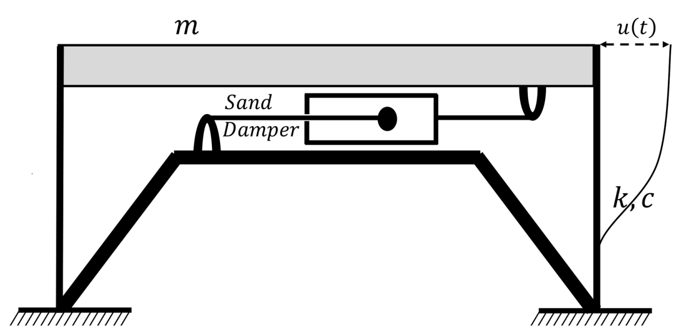

Fig. 8. Elastic SDOF structure equipped with a pressurized sand damper with strength $Q = \Pi_{SD}pR^2$ supported on a stiff chevron frame.

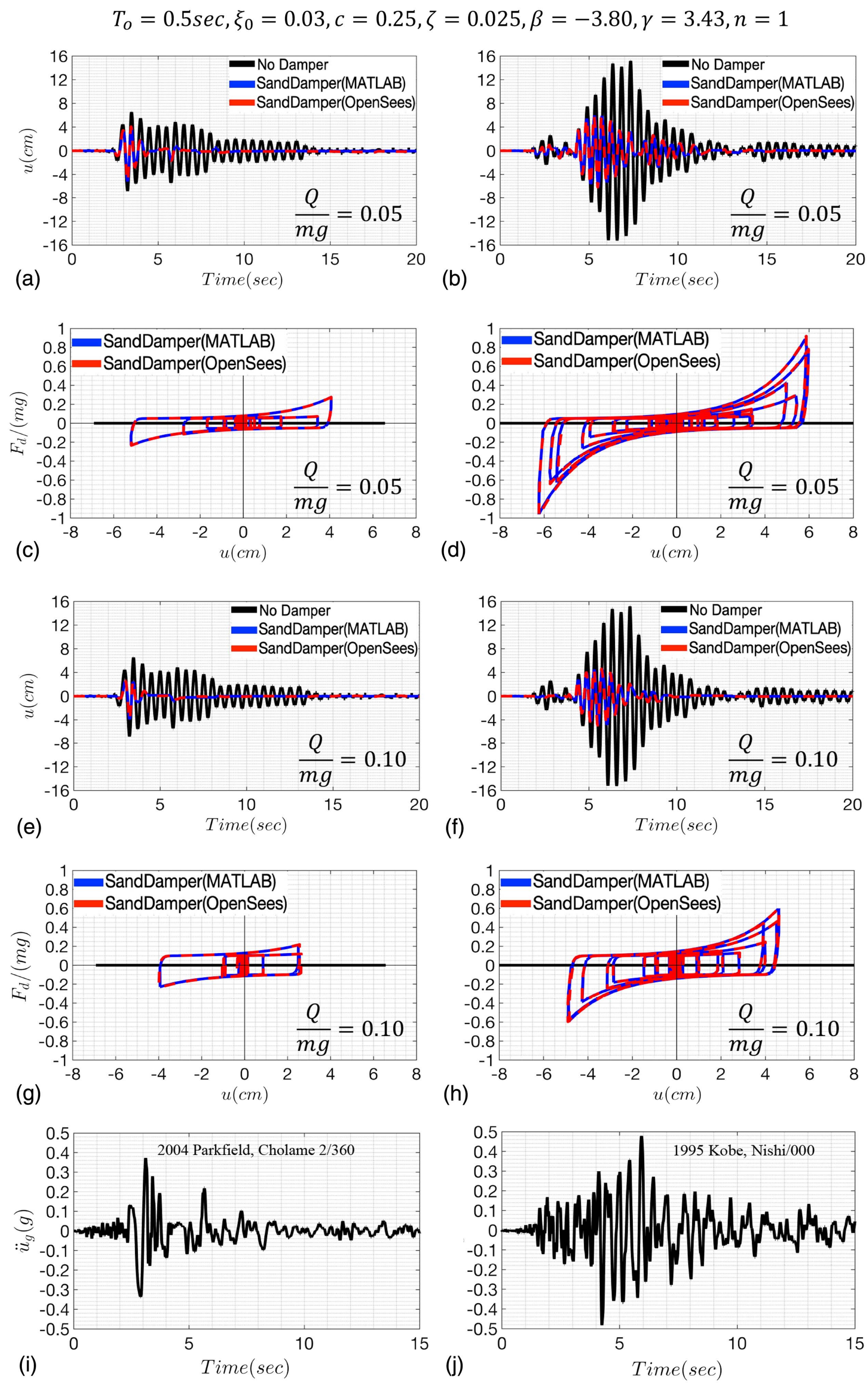

Fig. 9. (a, b, e, and f) Displacement time histories of the SDOF structure shown in Fig. 8 without damper (solid lines with larger amplitudes); and with damper (suppressed lines) together with (c, d, g, and h) the corresponding force-displacement loops of the supplemental pressurized sand damper when subjected to (i) the Cholame 2/360 ground motion recorded during the 2004 Parkfield earthquake; and (j) the Nishi/000 ground motion recorded during the 1995 Kobe earthquake. The numerical solutions obtained with the C++ algorithm implemented in OpenSees and with MATLAB are essentially identical.

of loading of an untested bearing than in subsequent cycles (Thompson et al. 2000; Morgan et al. 2001). In the pressurized sand damper, as the sphere attached to the damper piston moves to larger strokes, it further compresses the sand toward the stroke end, and in subsequent cycles of the same amplitude, u_0, the moving sphere encounters less resistance, which translates to a milder pinching effect. This first-passage effect essentially vanishes after the first $3/4$ of the first cycle, as shown in Fig. 3.

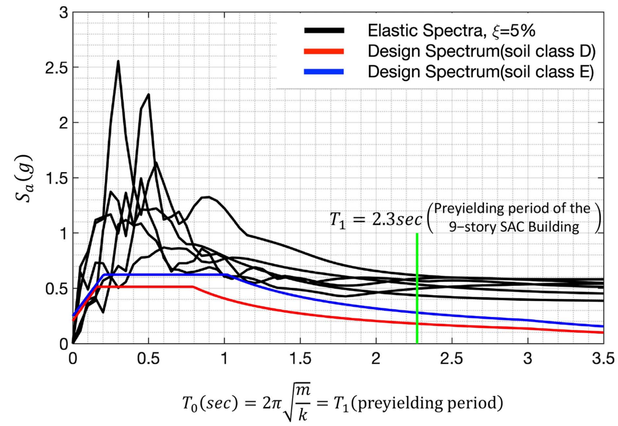

Fig. 10. Elastic response spectra of the six recorded ground motions used in this study together with the design elastic spectra for Soil classes D and E (ASCE 2013).

Development and Verification of an OpenSees Routine for Pressurized Sand Dampers

Given that the aim of the paper is to examine the response of multistory structures equipped with pressurized sand dampers, the first task is the development of a C++ routine that offers the force output from the nonlinear hysteretic model described by Eqs. (1) and (2), which was implemented in the open source structural analysis software OpenSees (McKenna et al. 2000). The developed C++ algorithm follows essentially the incremental formulation presented by Haukaas (2003). Accordingly, at time step t_{j+1}, the force output of the damper is

$$F_d(t_{j+1}) = Q[\mathrm{sgn}(\dot{u}(t_{j+1})) + \zeta z(t_{j+1})] \tag{4}$$

and the rate equation for $z(t_{j+1})$ is discretized by a backward Euler scheme as summarized in Appendix.

The verification of the C++ algorithm that was implemented in OpenSees is presented herein, with the response analysis of an elastic single-degree-of-freedom (SDOF) structure with mass m, stiffness k, and viscous damping c shown in Fig. 8 that is equipped with a pressurized sand damper with strength $Q = \Pi_{SD} pR^2$ supported on a noncompliant chevron frame. The SDOF elastic structure has natural frequency $\omega_0 = 2\pi/T_0 = \sqrt{k/m}$ and viscous damping ratio $\xi = c/2m\omega_0$ and is subjected to earthquake-induced excitation, $\ddot{u}_g(t)$. Dynamic equilibrium of the SDOF structure gives

$$m\ddot{u}(t) + c\dot{u}(t) + ku(t) + F_d(t) = -m\ddot{u}_g(t) \tag{5}$$

where $F_d(t)$ = hysteretic damping force offered by the pressurized sand damper given by Eq. (1). Upon dividing with the mass m, Eq. (5) in association with Eq. (1) gives

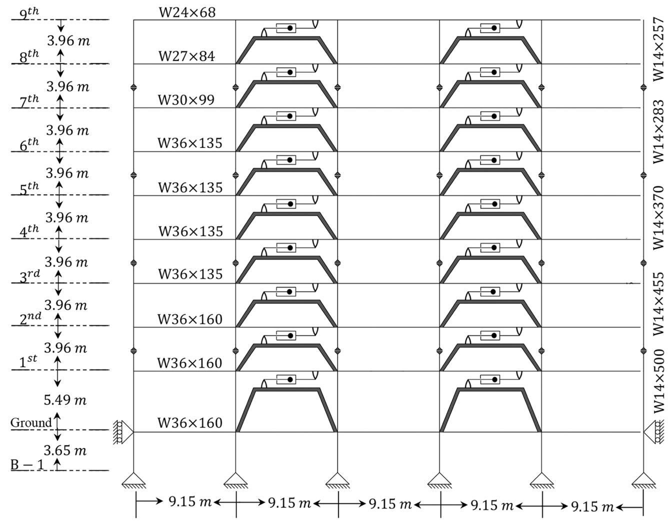

(a)

Columns (345 MPa)		Beams (248 MPa)	
• $B1-1^{st}$ level	W14 × 500	• Ground -2^{nd} level	W36 × 160
• $1^{st}-3^{rd}$ level	W14 × 455	• $3^{rd}-6^{th}$ level	W36 × 135
• $3^{rd}-5^{th}$ level	W14 × 370	• 7^{th} level	W30 × 99
• $5^{th}-7^{th}$ level	W14 × 283	• 8^{th} level	W27 × 84
• $7^{th}-9^{th}$ level	W14 × 257	• 9^{th} level	W24 × 68
Dimensions		**Seismic Mass**	
• Basement level height	3.65 m	Ground level	4.82×10^5 kg
• Ground level height	5.49 m	1^{st} level	5.05×10^5 kg
• $1^{st}-8^{th}$ level heights	3.96 m	$2^{nd}-8^{th}$ level	4.95×10^5 kg
• Bay width (all)	9.15 m	9^{th} level	5.35×10^5 kg

Restrains:
- Columns are pinned at base level.
- Structure is laterally restrained at 1^{st} level.
- Columns splices are at 1.83 m with respect to beam-to-column joint.

(b)

Fig. 11. (a) The 9-story moment-resisting steel frame designed for the SAC Phase II Project equipped at all levels with pressurized sand dampers supported on a noncompliant chevron frame; and (b) geometric and physical characteristics pertinent to the 9-story SAC building. The indicated seismic mass is the entire mass of each floor of the SAC building.

$$\ddot{u}(t) + 2\xi\omega_0\dot{u}(t) + \omega_0^2 u(t) + \frac{Q}{m}[\mathrm{sgn}[\dot{u}(t)] + \zeta z(t)] = -\ddot{u}_g(t) \tag{6}$$

where $z(t)$ = dimensionless internal variable offered by Eq. (2) and parameter $n = 1$. Accordingly, the state vector of the system $\{y(t)\}$ is expressed as

$$\{y(t)\} = \langle y_1(t), y_2(t), y_3(t)\rangle^T = \langle u(t), \dot{u}(t), z(t)\rangle^T \tag{7}$$

where superscript T = transpose of the line vector, $\langle\rangle$. The time-derivative state vector, $\{\dot{y}(t)\}$, is expressed by

$$\{\dot{y}(t)\} = \begin{Bmatrix} \dot{u}(t) \\ \ddot{u}(t) \\ \dot{z}(t) \end{Bmatrix} = \begin{Bmatrix} y_2(t) \\ -\ddot{u}_g(t) - 2\xi_o\omega_o y_2(t) - \omega_o^2 y_1(t) - \dfrac{Q}{m}[\mathrm{sgn}[y_2(t)] + \zeta y_3(t)] \\ \dfrac{1}{cR}[y_2(t) - \beta y_2(t)|y_3(t)|^n - \gamma|y_2(t)|y_3(t)|y_3(t)|^{n-1}] \end{Bmatrix} \tag{8}$$

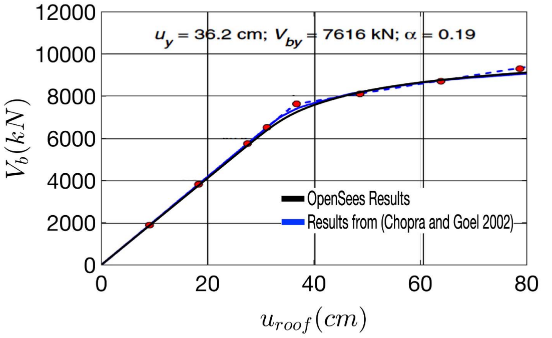

Fig. 12. Comparison of the captured pushover (base shear versus roof displacement) of the 9-story moment-resisting steel building in Fig. 11 with the results reported by Chopra and Goel (2002).

The numerical solution obtained with the C++ algorithm version 13.1.6 outlined in Appendix, and implemented in the open source software OpenSees (McKenna et al. 2000), is compared against the numerical solution obtained with MATLAB version R2020a in which the time derivative of the state vector $\{\dot{y}(t)\}$ offered by Eq. (8) is integrated with standard ordinary differential equations (ODE) solvers available in MATLAB.

Fig. 9 plots the relative-to-the-ground displacement response of the SDOF structure shown in Fig. 8 with $T_0 = 0.5$ s and $\xi = 0.03$ without and with a pressurized sand damper with $Q/\text{mg} = 0.05$ [Figs. 9(a–d)] and $Q/\text{mg} = 0.10$ [Figs. 9(e–h)] when subjected to the Cholame 2/360 ground motion recorded during the 2004 Parkfield, California, earthquake [Fig. 9(i)] and the Nishi-Akashi/000 ground motion recorded during the 1995 Kobe, Japan, earthquake [Fig. 9(j)].

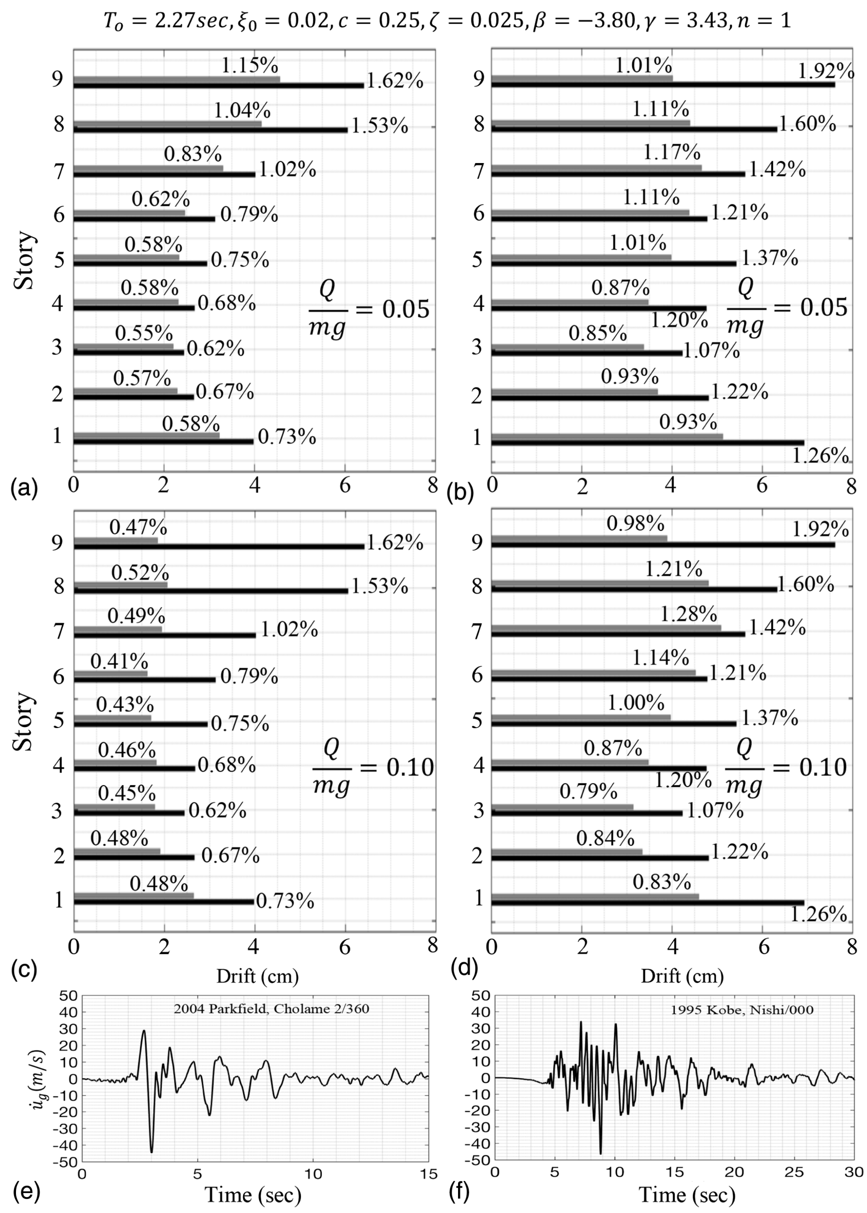

Fig. 13. Peak interstory displacements of the 9-story SAC steel building (heavy dark bars) without and (gray bars) with pressurized sand dampers with strength (a and b) $Q = 0.05$ mg; and (c and d) $Q = 0.10$ mg when subjected to (e) the Cholame 2/360 ground motion recorded during the 2004 Parkfield earthquake; and (f) the Nishi/000 ground motion recorded during 1995 Kobe, Japan, earthquake shown in Figs. 9(i and j).

J. Struct. Eng., 2022, 148(7): 04022071

The numerical solution obtained with the C++ algorithm implemented in OpenSees and with MATLAB are essentially identical. Fig. 9 indicates that the high-strength configuration of the damper ($Q/\mathrm{mg} = 0.1$) results in smaller displacements and also smaller peak forces because the pinching phenomenon is less pronounced at smaller displacements.

The seismic response analysis of the 9-story SAC building that follows in this study uses the six strong ground motions appearing in Figs. 9(i and j), 15(g and h), and 17(g and h). The elastic response spectra for viscous damping ratio $\xi = 5\%$ of these six historic ground motions exceed by far at the preyielding period of the structure, $T_1 = 2.3$ s, the design elastic spectra for Soil classes D and E (ASCE 2013) as shown in Fig. 10. For instance, the lower earthquake spectral value is 2.2 times larger than the Class D design spectral value and 1.9 times larger than the Class E design spectral value.

Seismic Response of the 9-Story SAC Building Equipped with Pressurized Sand Dampers

The 9-story SAC building (Gupta and Krawinkler 1998; Chopra and Goel 2002) was designed to meet the seismic code (pre-Northridge earthquake) and represents typical medium-rise buildings designed for the greater area of Los Angeles, California.

This moment-resisting steel building is 40.82 m tall with nine stories above ground level and a basement, as shown in Fig. 11. The bays are 9.15 m wide, with five bays in the north-south (N-S) and east-west (E-W) directions. The floor-to-floor height of each story is 3.96 m, except for the basement and first floor, which are 3.65 and 5.49 m, respectively, as shown in Fig. 11. Column splices are on the first, third, fifth, and seventh floors and located 1.83 m above the beam-column joint. The column bases are modeled as pinned

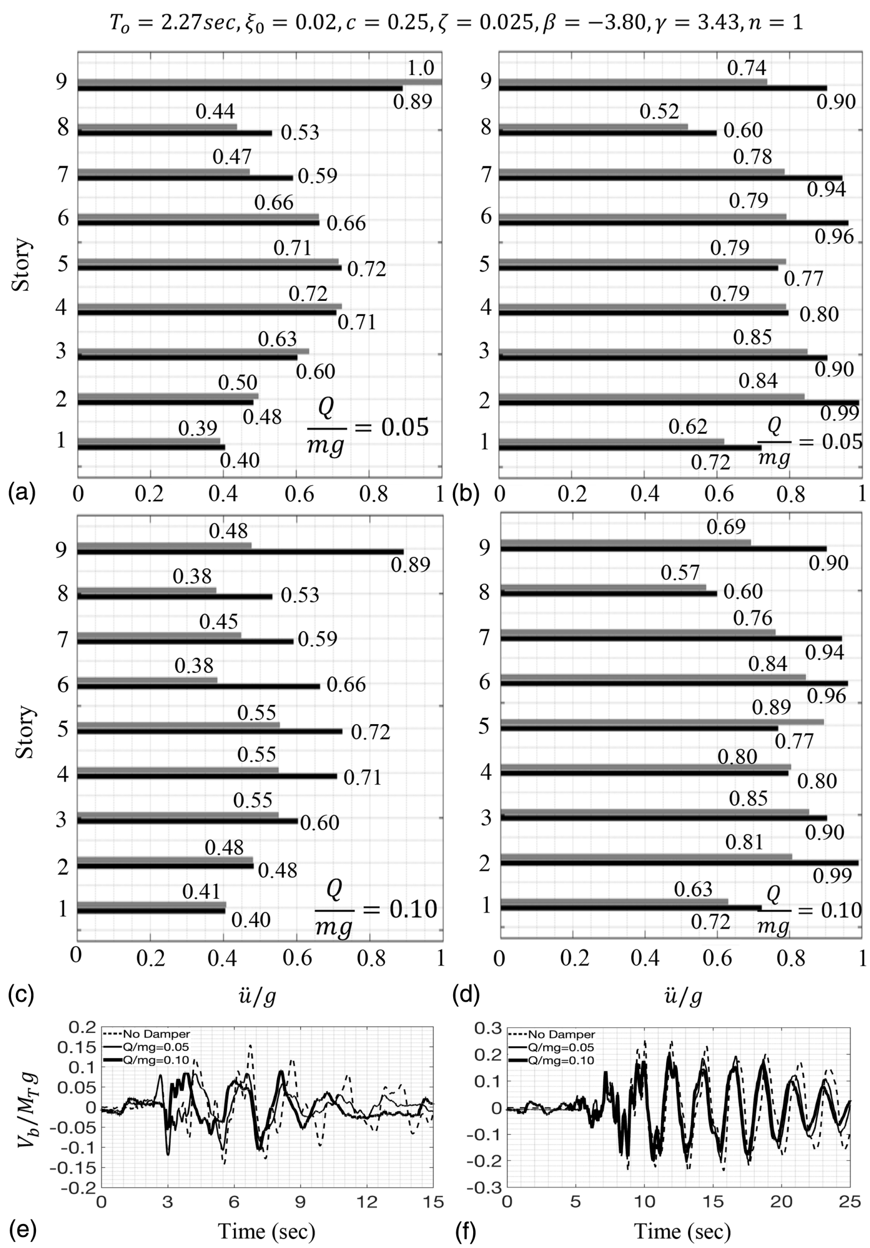

Fig. 14. Peak floor accelerations of the 9-story SAC steel building (heavy dark bars) without and (gray bars) with pressurized sand dampers with strength (a and b) $Q = 0.05$ mg; (c and d) $Q = 0.10$ mg when subjected to the Cholame 2/360 ground motion recorded during the 2004 Parkfield earthquake and the Nishi/000 ground motion recorded during the 1995 Kobe, Japan earthquake [(a–d), respectively]; and (e and f) computed base shear of the (dashed lines) undamped and (solid lines) damped 9-story SAC building.

J. Struct. Eng., 2022, 148(7): 04022071

connections, and it is assumed that the surrounding soil and concrete foundation walls are restraining the structure in the horizontal direction at the ground level. The columns are 345-MPa-wide-flange steel sections, and the floor beams are composed of 248-MPa-wide-flange steel sections. All beam column connections of the frames are rigid except for the corner columns, which are pinned in order to avoid biaxial bending of the members. In this study, the exterior frame in the N-S direction is chosen for the two-dimensional (2D) validation of our planar analysis.

The nonlinear response of the 9-story multi-degree-of-freedom (MDOF) structure is computed with the nonlinear built-in model *Steel01* in OpenSees, which is essentially a bilinear model, at the stress-strain level. Accordingly, we have used an elastic modulus of $E = 210$ GPa, a strain hardening ratio (postyield to elastic, preyield modulus ratio), $a = 0.03$, and a yield strength, $\sigma_y = 248$ MPa for beams, and $\sigma_y = 345$ MPa for columns.

Fig. 12 plots the computed pushover curve (base shear versus roof displacement) of the 9-story moment-resisting steel building without the hysteretic damper, which is essentially identical with the pushover curve presented in past investigations (Gupta and Krawinkler 1998; Chopra and Goel 2002). The resulting preyielding period is $T_1 \approx 2.3$ s. The C++ routine summarized in Appendix that returns the force output of the pressurized sand damper given the time history of the interstory displacement was implemented in OpenSees for the response analysis of the 9-story moment-resisting SAC building equipped with pressurized sand dampers shown in Fig. 11.

Fig. 6 indicates that depending on the stroke amplitude ($u_0 = 4.0, 6.0$, and 8.0 cm), neighboring yet different values of the parameters β, γ, and ζ of the proposed Bouc-Wen hysteretic model, as described by Eqs. (1) and (2), are needed due to the first-passage effect on the moving sphere to best fit the recorded

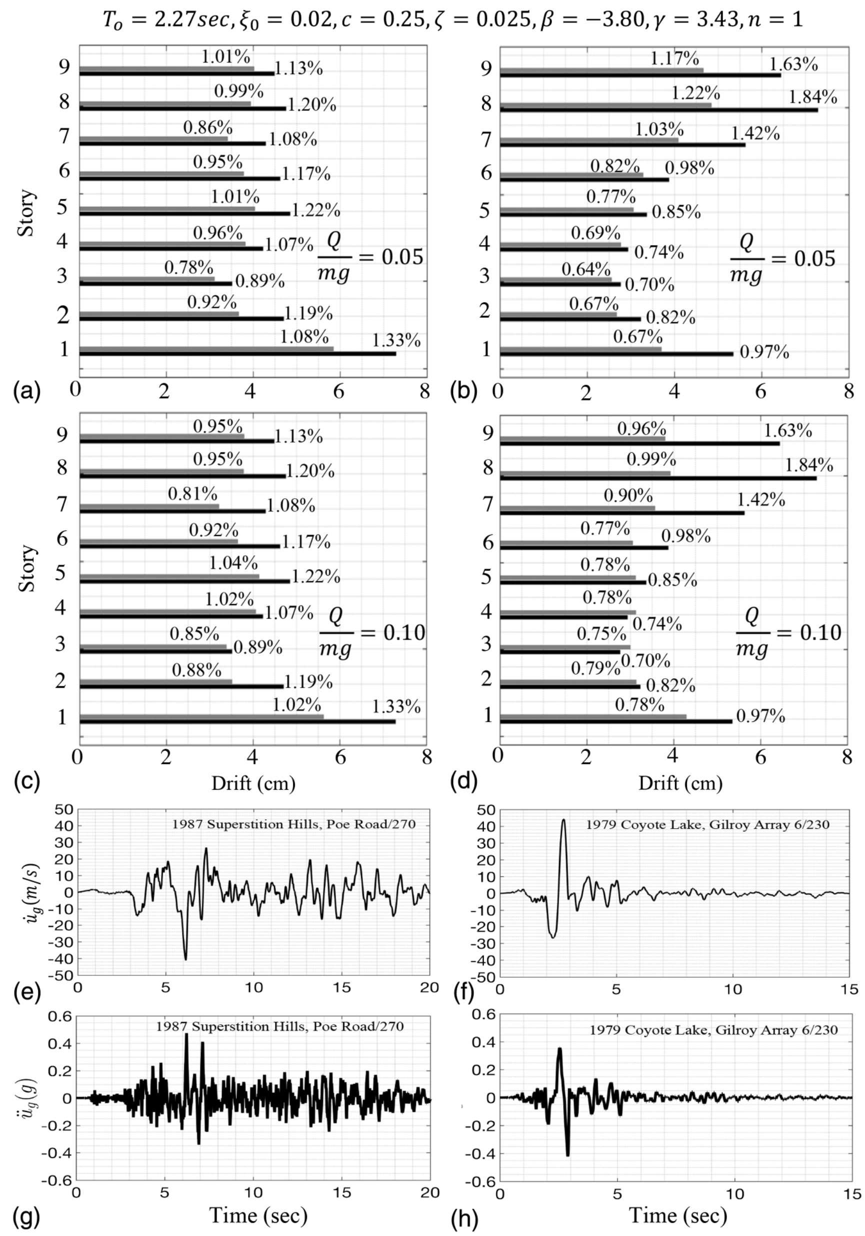

Fig. 15. Peak interstory displacements of the 9-story SAC steel building (heavy dark bars) without and (gray bars) with pressurized sand dampers with strength (a and b) $Q = 0.05$ mg; and (c and d) $Q = 0.10$ mg when subjected to (e–h) the Poe Road/270 ground motion recorded during 1987 Superstition Hills earthquake and the Gilroy Array 6/230 ground motion recorded during the 1979 Coyote Lake earthquake.

J. Struct. Eng., 2022, 148(7): 04022071

force-displacement loops at each given stroke amplitude. When the values of parameters β, γ, and ζ identified for a lower stroke amplitude (say, $u_0 = 4.0$ cm) are used to model the damper response at higher amplitudes (say, $u_0 = 6.0$ or 8.0 cm), then a more pronounced pinching effect is produced by the hysteretic model at higher amplitudes. Accordingly, in order to be on the conservative side and avoid the generation of unrealistic large hysteretic forces, at every analysis the values of the model parameters β, γ, and ζ are those associated with displacement amplitudes at or above the interstory displacements of the building when equipped with dampers. As an example, Figs. 13(a and b) shows with heavy dark bars the interstory displacement of the 9-story SAC steel frame without dampers when subjected to the Cholame 2/360 ground motion recorded during the 2004 Parkfield, California, earthquake. Given that the interstory displacements at the eighth and ninth level marginally exceed 6.0 cm, whereas all the other interstory displacements are below 6.0 cm, the analysis when the 9-story SAC building is equipped with dampers uses the parameters $\beta = -3.80$, $\gamma = 3.43$, and $\zeta = 0.025$ identified from cyclic testing of the damper with stroke amplitude $u_0 = 6.0$ cm [see Fig. 6(b)]. Figs. 13(a and b) shows that interstory displacements of the 9-story SAC building when equipped with pressurized sand dampers (gray bars) are all below 6.0 cm, therefore the choice of the parameter values $\beta = -3.80$, $\gamma = 3.43$, and $\zeta = 0.025$ is appropriate. The same applies to the response analysis of the 9-story SAC building equipped with pressurized sand dampers shown in Figs. 13(c and d) when subjected to the Nishi-Akashi/000 ground motion recorded during the 1995 Kobe, Japan, earthquake. Fig. 13 shows that the pressurized

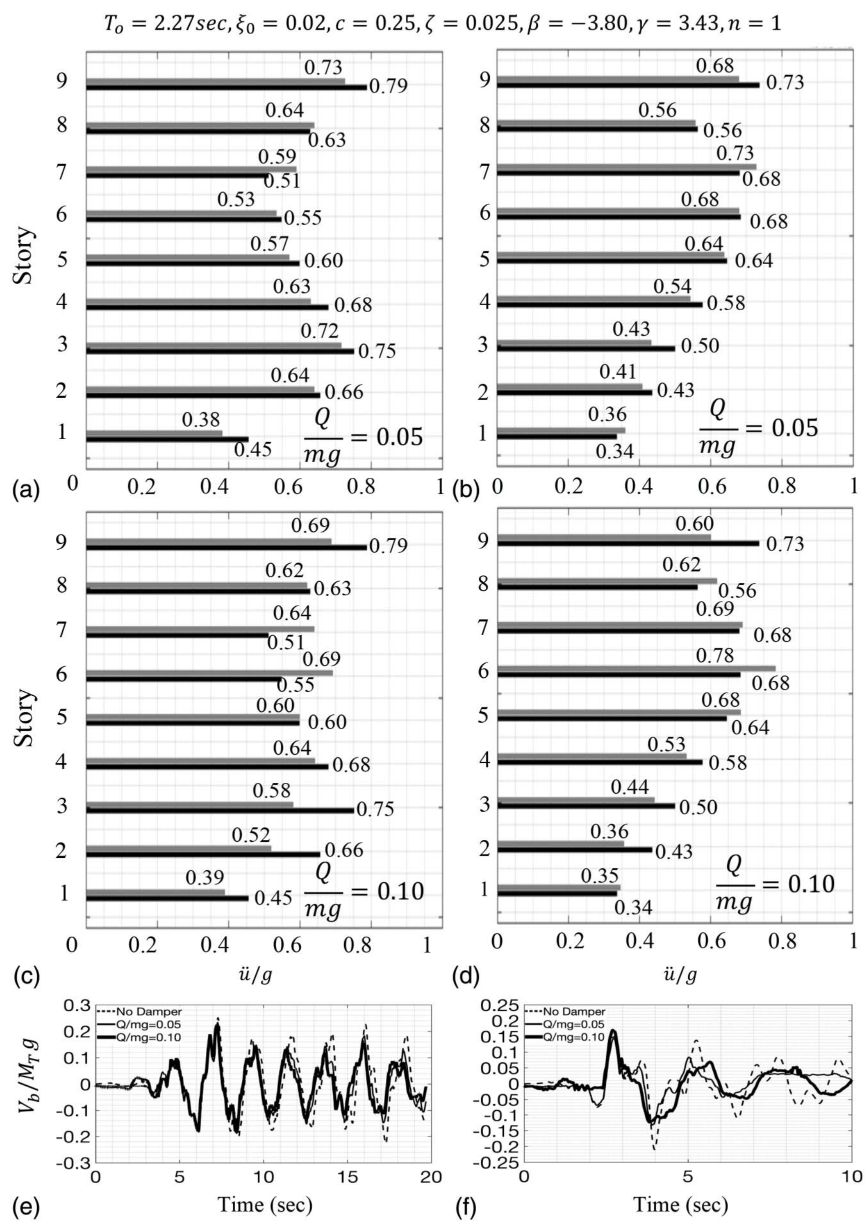

Fig. 16. Peak floor accelerations of the 9-story SAC steel building (heavy dark bars) without and (gray bars) with pressurized sand dampers with strength (a and b) $Q = 0.05$ mg; (c and d) $Q = 0.10$ mg when subjected to the Cholame 2/360 ground motion recorded during the 1987 Superstition Hills earthquake and the Gilroy Array 6/230 ground motion recorded during the 1979 Coyote Lake earthquake [(a–d), respectively]; and (e and f) computed base shear of the (dashed lines) undamped and (solid lines) damped 9-story SAC building.

sand dampers are effective in reducing interstory displacements, and when their strength Q is 10% of the weight of their corresponding floors, all drifts are below 1% of the story height.

The peak floor accelerations of the 9-story SAC steel building when subjected to the two ground motions discussed in Fig. 13 are shown in Figs. 14(a–d), whereas Figs. 14(e and f) plots the corresponding base-shear time history of the undamped and damped SAC building. Figs. 14(a and b) indicates that when supplemental damping is provided, peak floor accelerations are reduced in most floors; nevertheless, the opposite happens in a small number of floors. The use of supplemental damping invariably reduces the base shears.

Figs. 15(a and b) shows with heavy dark bars the interstory displacements of the 9-story SAC steel frame without dampers when subjected to the Poe Road/270 ground motion recorded during the 1987 Superstition Hills, California, earthquake. All interstory displacements other than the one of the first level are below 6.0 cm; therefore, the analysis when the SAC building is equipped with pressurized sand dampers uses the parameters $\beta = -3.80$, $\gamma = 3.43$, and $\zeta = 0.025$ identified from cyclic testing of the damper with stroke amplitude $u_0 = 6.0$ cm [see Fig. 6(b)]. Figs. 15(a and b) shows that the interstory displacements of the 9-story SAC building when equipped with pressurized sand dampers (gray bars) are all below 6.0 cm, therefore the aforementioned choice of parameters β, γ, and ζ is appropriate. The same applies to the response analysis of the 9-story SAC building with pressurized sand dampers shown in Figs. 15(c and d) when subjected to the Gilroy Array 6/230 ground motion recorded during the 1979 Coyote Lake, California, earthquake. Fig. 15 shows that the pressurized sand dampers are effective in reducing interstory drifts at or below 1% of the story height. Fig. 15 shows that the base shears of the damped 9-story SAC building are invariably lower than when the building is undamped.

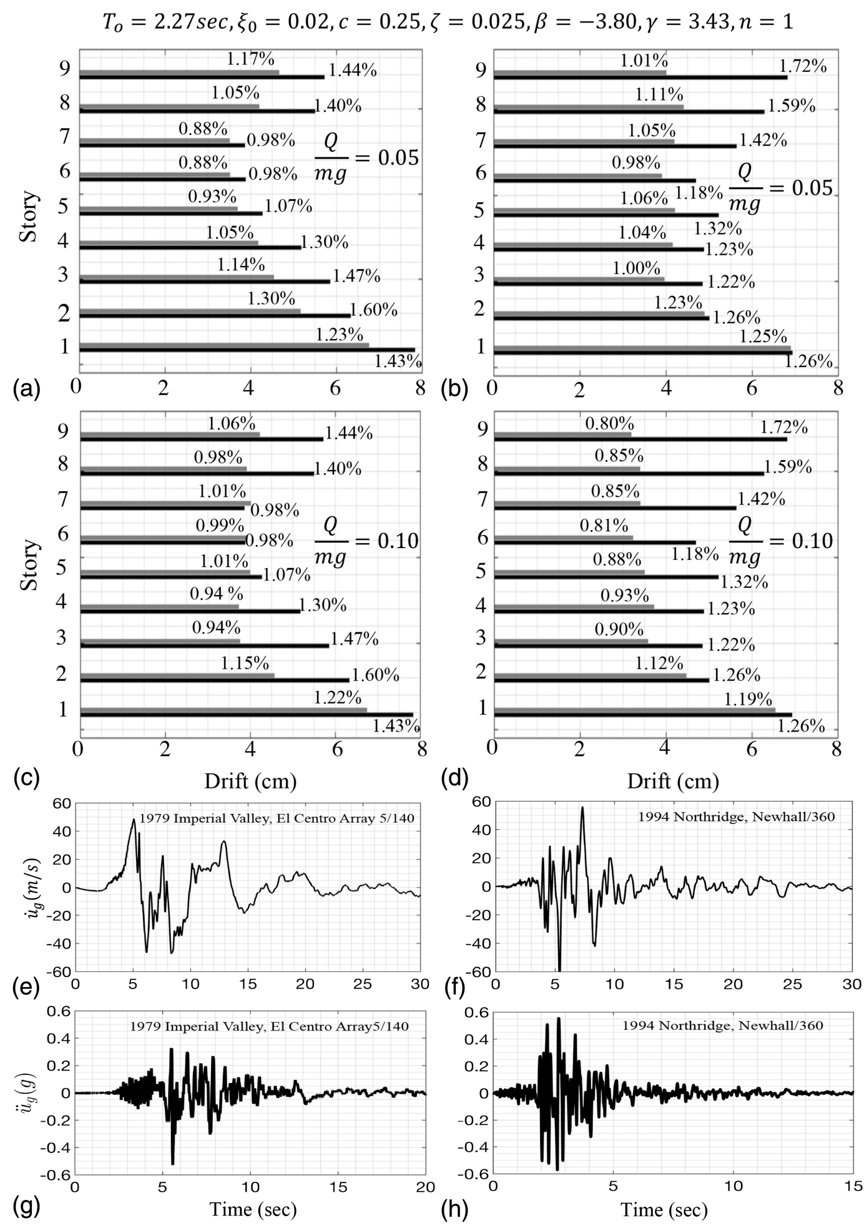

Fig. 17. Peak interstory displacements of the 9-story SAC steel building (heavy dark bars) without and (gray bars) with pressurized sand dampers with strength (a and b) $Q = 0.05$ mg; and (c and d) $Q = 0.10$ mg when subjected to (e and g) the El Centro Array 5/140 ground motion recorded during the 1979 Imperial Valley earthquake; and (f and h) the Newhall/360 ground motion recorded during 1994 Northridge earthquake.

J. Struct. Eng., 2022, 148(7): 04022071

The peak floor accelerations of the 9-story SAC steel building when subjected to the two ground motions discussed in Fig. 15 are shown in Figs. 16(a–d), whereas Figs. 16(e and f) plots the base-shear histories of the undamped and damped SAC building. Again, Fig. 16 indicates that supplemental damping in general reduces floor acceleration; nevertheless, the opposite happens in a small number of floors.

Fig. 17 shows the interstory displacements of the 9-story SAC steel frame without and with dampers when subjected to the El Centro Array 5/140 ground motion recorded during the 1979 Imperial Valley earthquake [Figs. 17(a, c, e, and g)] and the Newhall/360 ground motion recorded during 1994 Northridge earthquake [Figs. 17(b, d, f, and h)]. Again, the pressurized sand dampers with strength $Q_i = 0.05$ or $0.10\ \mathrm{m}_1\,\mathrm{g}$ are effective in suppressing interstory drifts except at the first level, which experiences drifts of the order of 1.2% of the floor's height level when the damper strength $Q_1 = 0.10\ \mathrm{m}_1\,\mathrm{g}$. In this case, at the first-floor dampers with strengths larger than $Q_1 = 0.10\ \mathrm{m}_1\,\mathrm{g}$ need to be installed to reduce the first-story displacement below 1% of the floor height. The base shears of the 9-story SAC building with supplemental damping are invariably lower than when the building is undamped.

The peak floor accelerations of the 9-story SAC steel building when subjected to the two ground motions discussed in Fig. 17 are shown in Figs. 18(a–d), whereas Figs. 18(e and f) plots the time history of the base shears. Again, as previously discussed, supplemental damping produces mixed results on floor accelerations; nevertheless, in most floors peak accelerations are reduced.

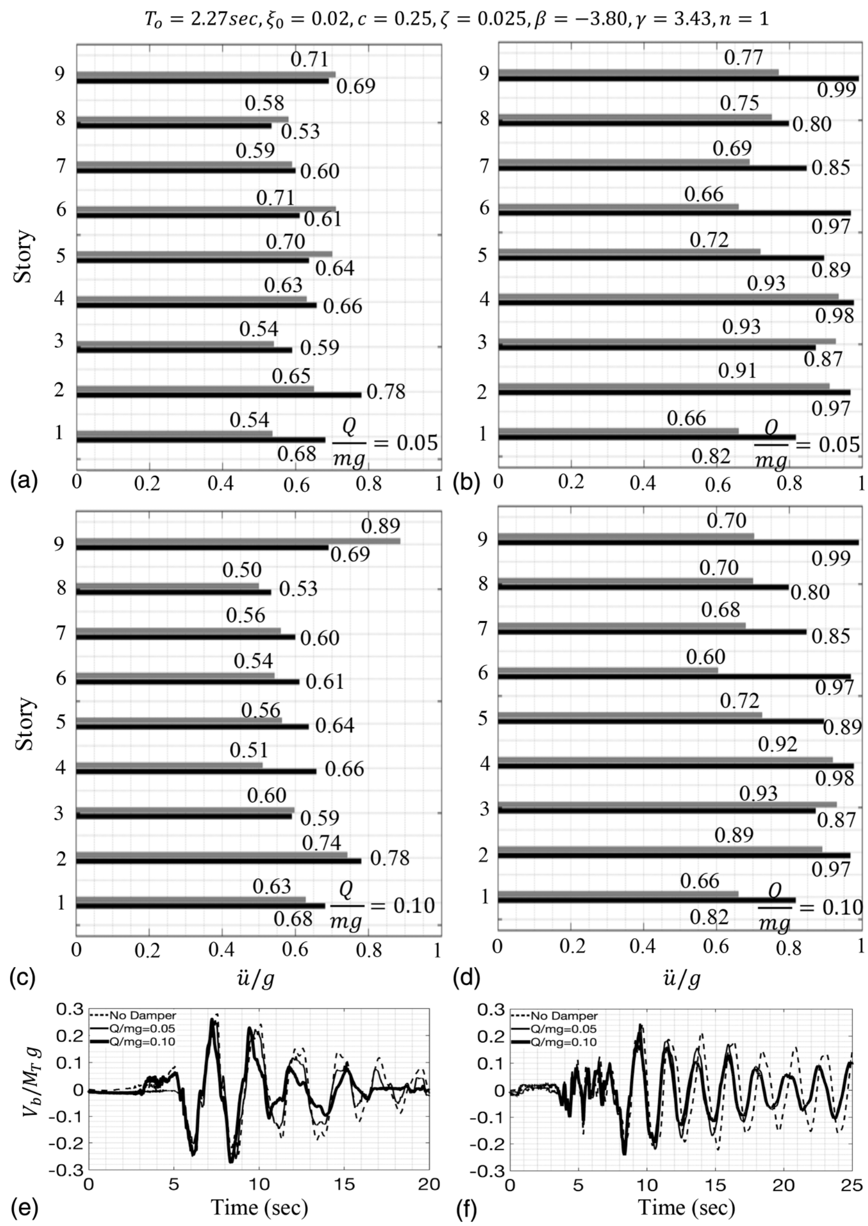

Fig. 18. Peak floor accelerations of the 9-story SAC steel building (heavy dark bars) without and (gray bars) with pressurized sand dampers with strength (a and b) $Q = 0.05$ mg; and (c and d) $Q = 0.10$ mg when subjected to the El Centro Array 5/140 ground motion recorded during the 1979 Imperial Valley earthquake and the Newhall/360 ground motion recorded during 1994 Northridge earthquake [(a–d), respectively]; and (e and f) computed base shear of the (dashed lines) undamped and (solid lines) damped 9-story SAC building.

J. Struct. Eng., 2022, 148(7): 04022071

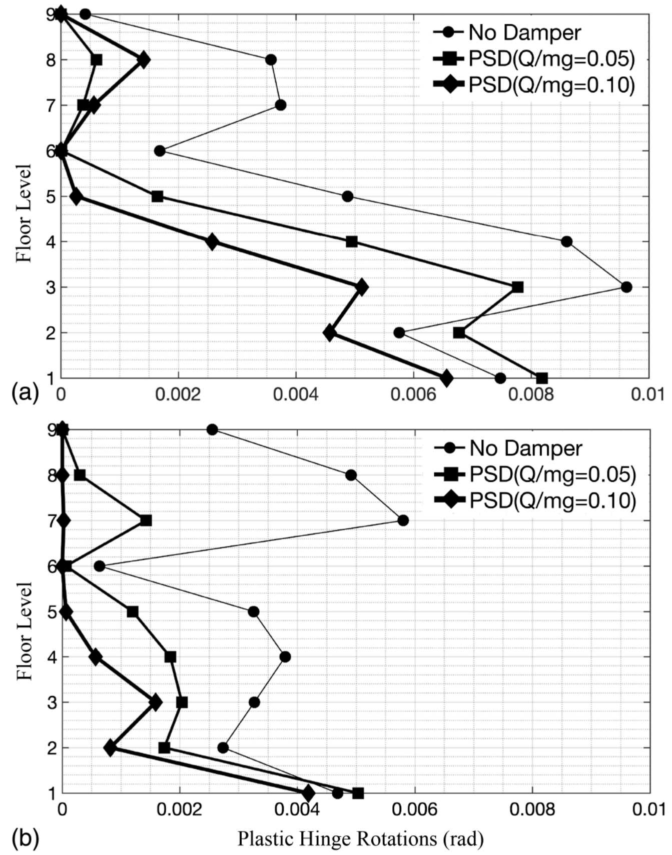

Fig. 19. Beam (at exterior columns) peak plastic hinge rotations of the 9-story SAC steel building without and with pressurized sand dampers with strength $Q = 0.05$ mg (squares) and $Q = 0.10$ mg (diamonds) when subjected to (a) the El Centro Array 5/140 ground motion recorded during the 1979 Imperial Valley earthquake; and (b) the Newhall/360 ground motion recorded during 1994 Northridge earthquake.

To this end, in addition to floor drifts, floor accelerations, and base shears, the response analysis presented herein computes peak values of the plastic hinge rotations of the beams at all levels of the 9-story moment-resisting frame shown in Fig. 11. The computed peak plastic hinge rotations of the beams that connect to the exterior columns on the left side of the frame are presented in Fig. 19 by following the presentation style of plastic hinge rotation profiles introduced in the seminal work of Gupta and Krawinkler (1998). Plastic hinge rotations of structural members can be directly obtained with the OpenSees open source platform by passing the *plasticDeformation* argument to the *Element recorder* command (Scott 2007).

Fig. 19 plots the profiles of the peak plastic hinge rotations of the beams that meet the exterior columns on the left of Fig. 11 (which also indicates the floor levels) when the structure is subjected to the El Centro Array 5/140 ground motion [Fig. 19(a)] and the Newhall/360 ground motion [Fig. 19(b)]. Fig. 19 shows that supplemental hysteretic damping from pressurized sand dampers with strength of the order of 10% of the weights of their corresponding floors reduces appreciably the peak plastic hinge rotations throughout the height of the 9-story moment-resisting building. At the same time, it needs to be recognized that plastic hinge formation at the lower-story columns is challenging to control, and large values of supplemental damping are needed to achieve reduction of hinge rotations.

Conclusions

The need to limit inelastic deformations and damage during the earthquake shaking of multistory buildings has prompted during the last four decades the use of supplemental energy dissipation devices. At present viscous fluid dampers and BRBs have emerged as the two types of passive energy dissipation devices that enjoy the widest implementations.

This paper investigates the seismic response analysis of the 9-story SAC building when equipped with pressurized sand dampers—a new type of low-cost, sustainable energy dissipation devices where the material enclosed within the damper housing is pressurized sand. The strength of the pressurized sand damper is proportional to the externally exerted pressure on the sand via prestressed steel rods and can be adjusted at will by monitoring the axial strains on the steel rods with standard inexpensive strain gauges. The strong pinching behavior of the pressurized sand damper is characterized with a previously developed three-parameter Bouc-Wen hysteretic model that in this work is implemented in the open source code OpenSees with a C++ algorithm and is used to analyze the seismic response of yielding buildings.

The inelastic response analysis study used six strong recorded ground motions that exceed the design response spectrum for all soil categories at the preyielding period of the 9-story SAC building. The paper concludes that pressurized sand dampers with strengths of the order of 5%–10% of the weights of corresponding floors are capable to keep interstory drifts of the 9-story SAC building at or below 1%. The implementation of pressurized sand dampers also reduces peak floor accelerations in most floors; however, the opposite happens in selective floors. The occasional exceedance of the peak acceleration at a given floor when supplemental damping is used does not follow any identified pattern. The base shears of the damped 9-story SAC building are invariably lower than when the building is not equipped with supplemental dampers. Finally, the paper shows that supplemental hysteretic damping from pressurized sand dampers with strengths of the order of 10% of the weights of their corresponding floors reduces appreciably peak plastic hinge rotations throughout the height of the 9-story moment-resisting building.

Appendix. Modeling the Pressurized Sand Damper in the Open Source Code OpenSees (McKenna et al. 2000)

The procedure implemented in OpenSees to model the hysteretic damper described by Eqs. (1) and (2) is summarized in Appendix.

While $\left(|z_{j+1}^{\text{old}} - z_{j+1}^{\text{new}}| > \text{tol}\right)$

- Evaluate function $f(z_{j+1})$

$$\psi = \beta + \gamma \text{sgn}[(u_{j+1} - u_j) z_{j+1}] \tag{9}$$

$$\phi = 1 - |z_{j+1}|^n \psi \tag{10}$$

$$f(z_{j+1}) = z_{j+1} - z_j - \frac{\phi}{u_y}(u_{j+1} - u_j) \tag{11}$$

- Evaluate function derivatives (prime denotes derivative with respect to z_{j+1})

$$\phi' = -n|z_{j+1}|^{n-1} \text{sgn}(z_{j+1}) \psi - |z_{j+1}|^n \psi \tag{12}$$

$$f'(z_{j+1}) = 1 - \frac{\phi'}{u_y}(u_{j+1} - u_j) \tag{13}$$

- Obtain trial value in the Newton scheme

$$z_{j+1}^{\text{new}} = z_{j+1} - \frac{f(z_{j+1})}{f'(z_{j+1})} \tag{14}$$

- Update z_{j+1} (and store the old value for the convergence check)

$$z_{j+1}^{\text{old}} = z_{j+1} \quad \text{and} \quad z_{j+1} = z_{j+1}^{\text{new}} \tag{15}$$

Compute the force described in Eq. (1).

Data Availability Statement

All data, models, or code that support the findings of this study are available from the corresponding author upon reasonable request.

Acknowledgments

This study was funded by the National Science Foundation with Grant No. CMMI-2036131. The cyclic testing on the prototype sand dampers at exerted pressures of 3.0 and 5.0 MPa was conducted at the University of Patras, Greece, by Dr. E. Strepelias under the supervision of Professor S. Bousias, and their effort is gratefully acknowledged.

References

Aghagholizadeh, M., and N. Makris. 2018. "Earthquake response analysis of yielding structures coupled with vertically restrained rocking walls." *Earthquake Eng. Struct. Dyn.* 47 (15): 2965–2984. https://doi.org/10.1002/eqe.3116.

ASCE. 2013. *Minimum design loads for buildings and other structures*. ASCE/SEI 7-13. Reston, VA: ASCE.

Baber, T. T., and M. N. Noori. 1985. "Random vibration of degrading, pinching systems." *J. Eng. Mech.* 111 (8): 1010–1026. https://doi.org/10.1061/(ASCE)0733-9399(1985)111:8(1010).

Barenblatt, G. I. 1996. *Scaling, self-similarity, and intermediate asymptotics: Dimensional analysis and intermediate asymptotics*. Cambridge, UK: Cambridge University Press.

Beck, J. L., and R. I. Skinner. 1973. "The seismic response of a reinforced concrete bridge pier designed to step." *Earthquake Eng. Struct. Dyn.* 2 (4): 343–358. https://doi.org/10.1002/eqe.4290020405.

Black, C. J., I. D. Aiken, and N. Makris. 2002. *Component testing, stability analysis, and characterization of buckling-restrained unbounded braces*. Berkeley, CA: Pacific Earthquake Engineering Research Center, College of Engineering, Univ. of California, Berkeley.

Black, C. J., and N. Makris. 2006. *Viscous heating of fluid dampers under wind and seismic loading: Experimental studies, mathematical modeling and design formulae*. Berkeley, CA: Earthquake Engineering Research Center, Univ. of California, Berkeley.

Black, C. J., and N. Makris. 2007. "Viscous heating of fluid dampers under small and large amplitude motions: Experimental studies and parametric modeling." *J. Eng. Mech.* 133 (5): 566–577. https://doi.org/10.1061/(ASCE)0733-9399(2007)133:5(566).

Black, C. J., N. Makris, and I. D. Aiken. 2003. "Component testing and modeling of buckling restrained unbounded braces." In *Proc., Conf. of Behavior of Steel Structure in Seismic Areas-Stessa*. Boca Raton, FL: CRC Press.

Black, C. J., N. Makris, and I. D. Aiken. 2004. "Component testing seismic evaluation and characterization of buckling restrained braces." *J. Struct. Eng.* 130 (6): 880–894. https://doi.org/10.1061/(ASCE)0733-9445(2004)130:6(880).

Boardman, P. R., B. J. Wood, and A. J. Carr. 1983. "Union house: A cross braced structure with energy dissipators." *Bull. N. Z. Soc. Earthquake Eng.* 16 (2): 83–97. https://doi.org/10.5459/bnzsee.16.2.83-97.

Charalampakis, A. E., and V. K. Koumousis. 2008. "On the response and dissipated energy of Bouc–Wen hysteretic model." *J. Sound Vib.* 309 (3–5): 887–895. https://doi.org/10.1016/j.jsv.2007.07.080.

Charleson, A. W., P. D. Wright, and R. I. Skinner. 1987. "Wellington Central Police Station—Base isolation of an essential facility." In *Proc., Pacific Conf. on Earthquake Engineering*, 377–388. Wellington, New Zealand: New Zealand Society for Earthquake Engineering.

Chopra, A., and R. Goel. 2002. "A modal pushover analysis procedure for estimating seismic demands for buildings." *Earthquake Eng. Struct. Dyn.* 31 (3): 561–582. https://doi.org/10.1002/eqe.144.

Constantinou, M. C., and M. A. Adnane. 1987. *Dynamics of soil-base-isolated-structure systems: Evaluation of two models for yielding systems*. Philadelphia: National Science Foundation, Dept. of Civil Engineering, Drexel Univ.

Constantinou, M. C., T. T. Soong, and G. F. Dargush. 1998. *Passive energy dissipation systems for structural design and retrofit*. Buffalo, NY: Multidisciplinary Center for Earthquake Engineering Research.

Constantinou, M. C., and M. D. Symans. 1993. "Seismic response of structures with supplemental damping." *Struct. Des. Tall Build.* 2 (2): 77–92. https://doi.org/10.1002/tal.4320020202.

Fahnestock, L. A., J. M. Ricles, and R. Sause. 2007. "Experimental evaluation of a large-scale buckling-restrained braced frame." *J. Struct. Eng.* 133 (9): 1205–1214. https://doi.org/10.1061/(ASCE)0733-9445(2007)133:9(1205).

FEMA. 2000. "SAC venture guidelines development committee." Accessed June 1, 2000. https://www.nehrp.gov/pdf/fema350.pdf.

FEMA. 2006. *Techniques for the seismic rehabilitation of existing buildings*. FEMA-547. Washington, DC: FEMA.

Foliente, G. C., M. P. Singh, and M. N. Noori. 1996. "Equivalent linearization of generally pinching hysteretic, degrading systems." *Earthquake Eng. Struct. Dyn.* 25 (6): 611–629. https://doi.org/10.1002/(SICI)1096-9845(199606)25:6<611::AID-EQE572>3.0.CO;2-S.

Gupta, A., and H. Krawinkler. 1998. "Seismic demands for the performance evaluation of steel moment resisting frame structures." Ph.D. dissertation, Dept. of Civil and Environmental Engineering, Stanford Univ.

Hanson, R. D., and T. T. Soong. 2001. *Seismic design with supplemental energy dissipation devices*. Oakland, CA: Earthquake Engineering Research Institute.

Haukaas, T. 2003. *Finite element reliability and sensitivity methods for performance-based engineering*. Berkeley, CA: Univ. of California, Berkeley.

Kelly, J. M. 1997. *Earthquake-resistant design with rubber*. London: Springer.

Kelly, J. M., R. I. Skinner, and A. J. Heine. 1972. "Mechanisms of energy absorption in special devices for use in earthquake resistant structures." *Bull. N.Z. Soc. Earthquake Eng.* 5 (3): 63–88.

Langhaar, H. L. 1951. *Dimensional analysis and theory of models*. New York: Wiley.

Ma, F., H. Zhang, A. Bockstedte, G. C. Foliente, and P. Paevere. 2004. "Parameter analysis of the differential model of hysteresis." *J. Appl. Mech.* 71 (3): 342–349. https://doi.org/10.1115/1.1668082.

Makris, N. 1998. "Viscous heating of fluid dampers. I: Small amplitude motions." *J. Eng. Mech.* 124 (11): 1210–1216. https://doi.org/10.1061/(ASCE)0733-9399(1998)124:11(1210).

Makris, N., and C. J. Black. 2003a. *Dimensional analysis of inelastic structures subjected to near fault ground motions*. Berkeley, CA: Earthquake Engineering Research Center, Univ. of California, Berkeley.

Makris, N., and C. J. Black. 2003b. "Dimensional analysis of rigid-plastic and elastoplastic structures under pulse-type excitations." *J. Eng. Mech.* 130 (9): 1006–1018. https://doi.org/10.1061/(ASCE)0733-9399(2004)130:9(1006).

Makris, N., X. Palios, G. Moghimi, and S. Bousias. 2021. "Pressurized sand damper for earthquake and wind engineering: Design, testing, and characterization." *J. Eng. Mech.* 147 (4): 04021014. https://doi.org/10.1061/(ASCE)EM.1943-7889.0001902.

Makris, N., Y. Roussos, A. S. Whittaker, and J. M. Kelly. 1998. "Viscous heating of fluid dampers. II: Large-amplitude motions." *J. Eng. Mech.* 124 (11): 1217–1223. https://doi.org/10.1061/(ASCE)0733-9399(1998)124:11(1217).

Matier, P., and A. Ross. 2013. *Bay Bridge shock absorbers spring leak*. San Francisco: San Francisco Chronicle.

McKenna, F., G. L. Fenves, and M. H. Scott. 2000. *Open system for earthquake engineering simulation, version 2.5.0*. Berkeley, CA: Univ. of California, Berkeley.

Morgan, T., A. S. Whittaker, and A. Thompson. 2001. "Cyclic behavior of high-damping rubber bearings." In *Proc. 5th World Congress on Joints, Bearings and Seismic Systems for Concrete Structures.* Indianapolis: American Concrete Institute.

Sabelli, R., S. Mahin, and C. Chang. 2003. "Seismic demands on steel braced frame buildings with buckling-restrained braces." *Eng. Struct.* 25 (5): 655–666. https://doi.org/10.1016/S0141-0296(02)00175-X.

Scott, M. H. 2007. "Analytical sensitivity of plastic rotations in beam-column elements." *J. Struct. Eng.* 133 (9): 1341–1345. https://doi.org/10.1061/(ASCE)0733-9445(2007)133:9(1341).

Skinner, R., R. Tyler, A. Heine, and W. Robinson. 1980. "Hysteretic dampers for the protection of structures from earthquakes." *Bull. N. Z. Nat. Soc. Earthquake Eng.* 13 (1): 22–36. https://doi.org/10.5459/bnzsee.13.1.22-36.

Skinner, R. I., J. M. Kelly, and A. J. Heine. 1974. "Hysteretic dampers for earthquake-resistant structures." *Earthquake Eng. Struct. Dyn.* 3 (3): 287–296. https://doi.org/10.1002/eqe.4290030307.

Soong, T. T., and G. F. Dargush. 1997. *Passive energy dissipation systems in structural engineering*. New York: Wiley.

Symans, M. D., F. A. Charney, A. S. Whittaker, M. C. Constantinou, C. A. Kircher, M. W. Johnson, and R. J. McNamara. 2008. "Energy dissipation systems for seismic applications: Current practice and recent developments." *J. Struct. Eng.* 134 (1): 3–21. https://doi.org/10.1061/(ASCE)0733-9445(2008)134:1(3).

Thompson, A. C., A. S. Whittaker, G. L. Fenves, and S. A. Mahin. 2000. "Property modification factors for elastomeric seismic isolation bearings." In *Proc., 12th World Conference on Earthquake Engineering*. Upper Hutt, NZ: New Zealand Society for Earthquake Engineering.

Wada, A., E. Saeki, T. Takeuch, and A. Watanabe. 1989. *Development of unbonded brace*. Column Technical Publication No. 1151989.12. Tokyo: Nippon Steel.

Watanabe, A., Y. Hitomoi, E. Saeki, A. Wada, and M. Fujimoto. 1988. "Properties of braces encased in buckling-restraining concrete and steel tube." In *Proc., 9th World Conf. on Earthquake Engineering*. Tokyo: Japan Association for Earthquake Disaster Prevention.

Wen, Y. K. 1976. "Method for random vibration of hysteretic systems." *J. Eng. Mech. Div.* 102 (2): 249–263. https://doi.org/10.1061/JMCEA3.0002106.

Whittaker, A. S., I. D. Aiken, D. Bergman, P. W. Clark, J. Cohen, J. M. Kelly, and R. E. Scholl. 1993. "Code requirements for the design and implementation of passive energy dissipation systems." In *Proc., of ATC*. Redwood City, CA: Applied Technology Council.